J. Mt. Sci. (2018) 15(6): 1354-1370 e-mail: jms@imde.ac.cn http://jms.imde.ac.cn
https://doi.org/10.1007/s11629-017-4697-0

Landslide inventory and susceptibility modelling using geospatial tools, in Hunza-Nagar valley, northern Pakistan

Alam Sher BACHA[1*] http://orcid.org/0000-0002-1467-7405; e-mail: mian.alamsher@gmail.com

Muhammad SHAFIQUE[1] http://orcid.org/0000-0002-4063-6666; e-mail: shafique08@yahoo.com

Harald van der WERFF[2] http://orcid.org/0000-0002-2871-3913; e-mail: harald.vanderwerff@utwente.nl

* *Corresponding author*

1 National Centre of Excellance in Geology, University of Peshawar, Peshawar-25130, Pakistan

2 Faculty of Geo-Information Science and Earth Observation (ITC), University of Twente, Enschede 7500 AE, The Netherlands

Citation: Bacha AS, Shafique M, van der Werff H (2018) Landslide inventory and susceptibility modelling using geospatial tools, in Hunza-Nagar valley, northern Pakistan. Journal of Mountain Science 15(6). https://doi.org/10.1007/s11629-017-4697-0

Abstract: A comprehensive landslide inventory and susceptibility maps are prerequisite for developing and implementing landslide mitigation strategies. Landslide susceptibility maps for the landslides prone regions in northern Pakistan are rarely available. The Hunza-Nagar valley in northern Pakistan is known for its frequent and devastating landslides. In this paper, we have developed a landslide inventory map for Hunza-Nagar valley by using the visual interpretation of the SPOT-5 satellite imagery and mapped a total of 172 landslides. The landslide inventory was subsequently divided into modelling and validation data sets. For the development of landslide susceptibility map seven discrete landslide causative factors were correlated with the landslide inventory map using weight of evidence and frequency ratio statistical models. Four different models of conditional independence were used for the selection of landslide causative factors. The produced landslides susceptibility maps were validated by the success rate and area under curves criteria. The prediction power of the models was also validated with the prediction rate curve. The validation results shows that the success rate curves of the weight of evidence and the frequency models are 82% and 79%, respectively. The prediction accuracy results obtained from this study are 84% for weight of evidence model and 80% for the frequency ratio model. Finally, the landslide susceptibility index maps were classified into five different varying susceptibility zones. The validation and prediction result indicates that the weight of evidence and frequency ratio model are reliable to produce an accurate landslide susceptibility map, which may be helpful for landslides management strategies.

Keywords: Landslides; Inventory map; Susceptibility assessment; Northern Pakistan

Received: 27 September 2017
1st Revision: 13 November 2017
2nd Revision: 01 March 2018
Accepted: 20 March 2018

Introduction

Landslides are commonly occurring disasters in mountainous regions. They have a devastating impact on infrastructure and on human lives (Regmi et al. 2010). It is estimated that, worldwide, around 1016 deaths and economic losses of about 4 billion US$ occur due to landslides every year (CRED 2016). Landslide induced damages are increasing because of increasing urbanization, unplanned development, deforestation and effects of climate change (Kanungo et al. 2008). To mitigate the impact of landslides, a landslides inventory and susceptibility maps are of significant importance for developing and implementing landslides mitigation and management strategies

(Ahmed 2015; Basharat et al. 2016; Erener et al. 2016; Martha et al. 2013; Mohammady et al. 2012).

Development of a landslide inventory is the first step in landslide susceptibility mapping (Booth et al. 2009). Geographic Information Systems (GIS) and remote sensing are useful to develop landslide inventories and to evaluate the spatial and temporal distribution of landslides (Akbar and Ha 2011; Ayalew and Yamagishi 2005; Chalkias et al. 2014; Lee and Sambath 2006; Quan and Lee 2012; Reis et al. 2012). Landslide inventories are mainly developed through visual interpretation of satellite images and aerial photographs (Saba et al. 2010; Scaioni et al. 2014), but can also be developed using object based image classification (Lodhi 2011; Martha et al. 2010). The influence of causative factors such as topography, geology, tectonics, drainage, land cover/land use and anthropogenic activity are evaluated to determine the spatial distribution and density of landslides (Kamp et al. 2008), which is subsequently can be used for landslide susceptibility mapping.

Landslide susceptibility can be assessed by qualitative and quantitative techniques, that divide an area into different susceptibility classes (Fell et al. 2008). Statistical models are used for landslide susceptibility mapping (Mohammady et al. 2012); which includes fuzzy logic (Pradhan 2010; Wan et al. 2012), analytical hierarchy process (AHP) (Kayastha et al. 2013; Park et al. 2013), frequency ratio (Demir et al. 2013; Reis et al. 2012), index of entropy (Pourghasemi et al. 2012), neuro-fuzzy models (Pradhan 2010) and logistic regression model (Chau and Chan 2005; Lee and Choi 2004; Shahabi et al. 2015; Talaei 2014). Weight of evidence statistical modelling, which estimates the importance of evidential parameters using prior and posterior probability (Bonham-Carter 1994), is frequently used for landslide susceptibility mapping (Dahal et al. 2008a; Lee and Choi 2004; Pradhan 2010; Regmi et al. 2010).

The Karakoram and Himalaya mountain ranges in northern Pakistan are prone to frequent landslides. This is mainly due to the rugged terrain, seismic activity, highly weathered and fractured lithologies, steep climatic gradients ranging from glacial to hyper-arid and infrastructure development on unstable slopes (Derbyshire et al. 2001; Kamp et al. 2008; Khattak et al. 2010; Kumar et al. 2006; Panzera et al. 2015; Shafique et al. 2016; Shaw and Rahman 2015). Similarly, the Hunza-Nagar valley is situated in the Karakoram mountain region is frequently affected by landslides (Derbyshire et al. 2001). The presence of thrust faults, young and fractured lithologies and exposed geomorphology features like scree slopes, glaciofluvial moraine and the presence of unconsolidated material on steep slopes (Hewitt 1998) make the area prone to landsliding. In January 2010, a landslide occurred near Attabad village. The landslide costs the lives of twenty people, destroyed over three hundred houses, buried 19 km of the Karakorum highway and blocked the river Hunza, leading to a new natural lake that still exists today (Kargel et al. 2010).

In this study, we develop a landslide inventory using remote sensing image. We evaluate the spatial distribution of the landslides and develop a landslide susceptibility map using weight of evidence and frequency ratio modelling techniques.

1 Study Area

The study area is located in the Hunza-Nagar valley of the Gilgit Baltistan province, northern Pakistan (Figure 1). The elevation ranges from 1746 m to 7315 m above sea level, with an average slope of 45°. The lower Hunza valley is situated on the northern side of the Main Karakoram Thrust (MKT) fault. The geology of the area comprises four formations, namely the Southern Karakoram metamorphic Complex (SKm), the Hunza Plutonic Unit (HPU), the Shaksgam Formation (SF) and Quaternary (Q) Deposits (Searle et al. 1999). The SKm consists of Paragneises with interbanded pelites and amphibolites. The Shaksgam Formation is a subsection of northern Karakoram terrain (Searle et al. 1999) and includes Permian massive limestones. The HPU is a subsection of Karakoram batholith and contains plagioclase, quartz, biotite and hornblende (Searle et al. 1999). The Quaternary Deposits consist of alluvium deposits, unconsolidated conglomerate, sand stone, siltstone and loess (Searle and Khan 1996).

The Hunza-Nagar valley has a series of NE-dipping thrust faults and normal faults. These faults exerts side by side various tectono-

stratigraphic units against each other and increase in metamorphic grade in the region (Palin et al. 2012), that results foliation and fractures in the rocks. The geomorphology of the study area is comprised of glaciofluvial terraces, ancient glacier moraines, loose material of steep scree slopes, debris flow in the debris cone and colluvium deposit with dissected mountains, producing talus deposits at the base of high cliffs (Hewitt 1998) (Figure 2). The steep scree slopes containing loose

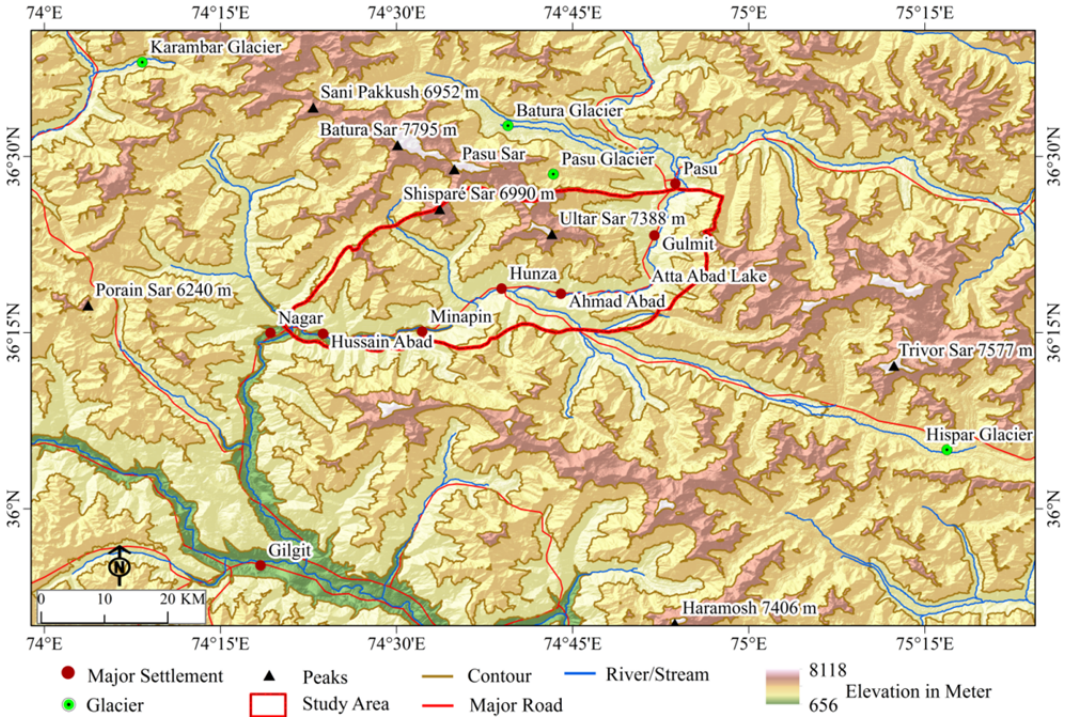

Figure 1 Location map of the study area.

Figure 2 A Google Earth image showing geomorphological features in the lower part of the Hunza-Nagar valley; scree slopes, terraces, fan terraces and old glacier moraines at Minapin and Nagar.

sediments are prone to sliding during heavy rainfall and seismic activity. The debris flow within debris cone can cause damages to the villages situated at the base of the scree slopes.

2 Materials and Methods

In this study, weights of evidence and frequency ratio modelling are used for landslide susceptibility mapping. The methodology adopted for this study is given in Figure 3. The data and data sources are shown in Table 1.

2.1 Landslide inventory

The landslide inventory was made by a visual interpretation of the SPOT-5 satellite image with a spatial resolution of 2.5 meter. Landslides can be detected in satellite images by spectral (color) variations and the shape of scarps (Chauhan et al. 2010; Sarkar et al. 2008). For 3D visualization, a natural color composite, i.e. a red, green and blue band combination, of the image was overlaid on a Shuttle Radar Topography Mission (SRTM) DEM with 30 m resolution, following Haeberlin et al.

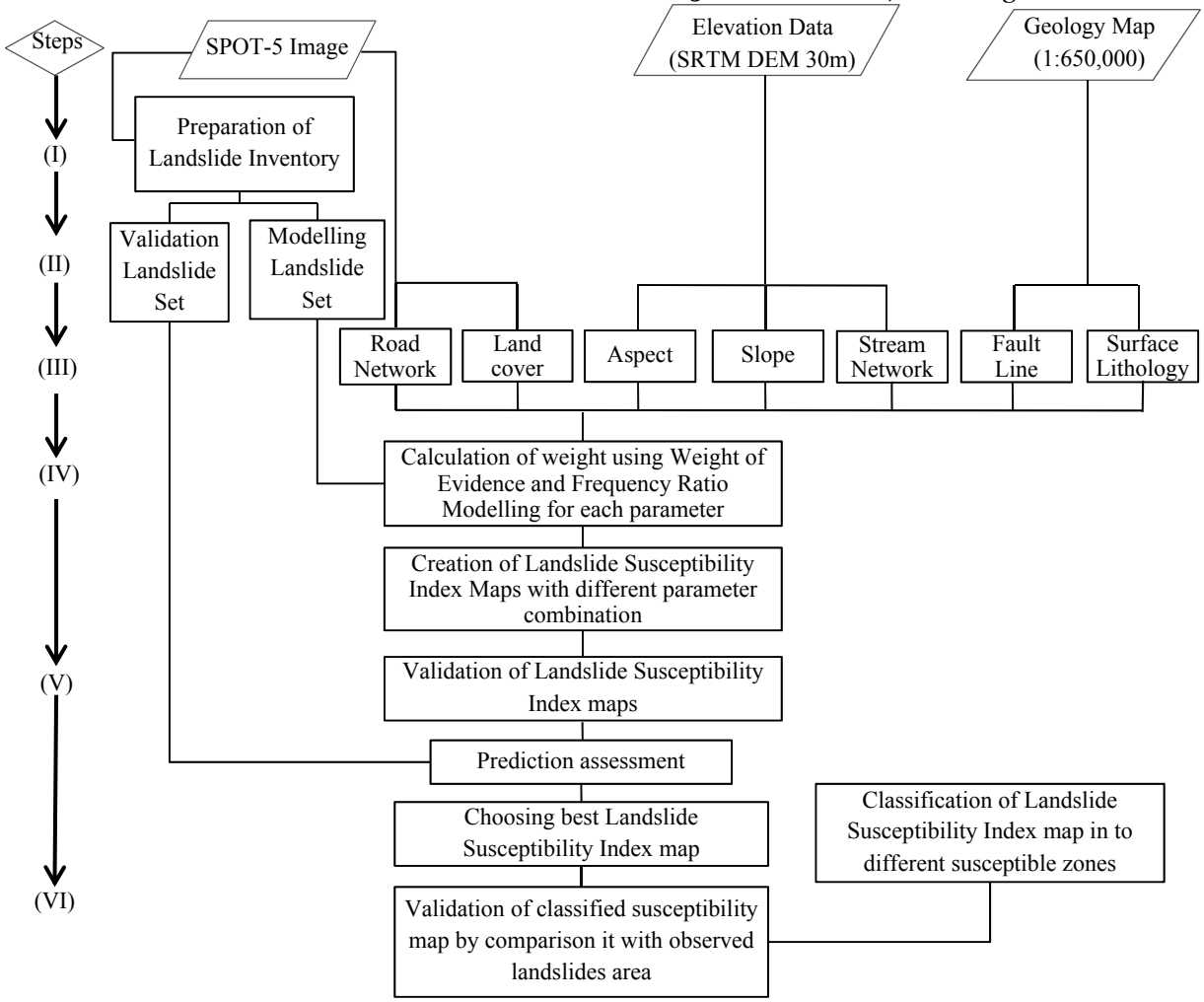

Figure 3 Methodology adopted for study.

Table 1 Data and data source used in this study

Data	Factors	Scale / resolution	Source
SPOT-5 Satellite Images	Landslide inventory Land cover/land use Road network	2.5 meter	Space and Upper Atmospheric Research Commission Pakistan (CNES)
DEM (SRTM)	Slope and Aspect Stream Network	30 meter	Shuttle Radar Topography Mission (USGS 2015).
Geological Map	Geology Units Fault lines	1:650,000	(Searle and Khan 1996)

(2004) (Figure 4). The landslide inventory was subsequently verified in the field and landslides outlines were adjusted if needed. The landslide inventory was then divided into modelling (80%) and a validation (20%) set.

2.2 Landslide controlling factors

The landslide controlling factors listed below were prepared in ArcGIS 10.2.2:

Slope and Aspect: Terrain slope and aspect were computed from the SRTM DEM. To evaluate the influence of slope angle on landslide distribution, the slope angle map was classified into seven classes, following (Dahal et al. 2008b), and the terrain aspect was divided in to 9 classes (Table 2).

Land cover: A land cover map was developed from the SPOT-5 image through supervised classification using the Maximum Likelihood Classification algorithm. To evaluate the impact of the land cover on landslides activity, the land cover of the study area was classified in six different classes (Table 2). Subsequently, the land cover map was verified in the field. The overall accuracy of the land cover map appeared to be 88.5%. Landslide scarps were assigned to the "barren" class. The classes "water" and "glacier" were not considered for analysis, because they do not expose land cover that could influence landslide occurrences.

Geology and faults: Fault lines and four geological formations were digitized from the geological map; the resulting classes are shown in Table 2. The names of the geological formations were explained in the study area section above. Six classes of distance to fault line were generated,

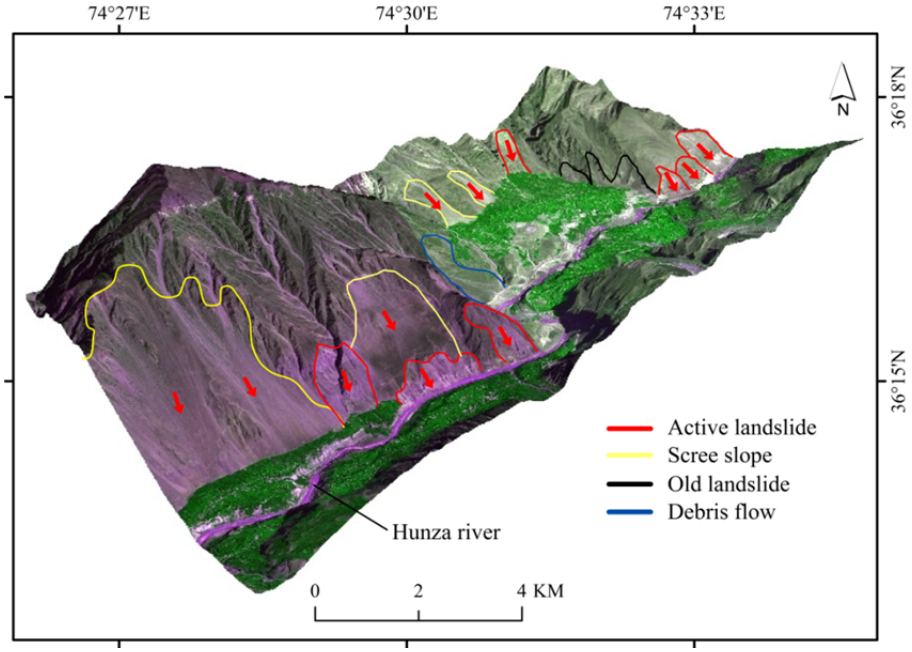

Figure 4 Shows a 3D visualization of the SPOT-5 true color composite image overlaid on the SRTM DEM. Showing landslides in the study area.

Table 2 Landslide controlling factors with classes used for evaluating the importance of each causative factor

Factors	Classes					
Geology	Glacier	SKm	HPU	SF	Q	
Land Cover	Agriculture	Barren	Forest	Glacier	Grass	Water
Slope (°)	< 10 > 60	11-20	21-30	31-40	41-50	51-60
Proximity to Fault (meter)	<10	11-20	21-50	51-100	101-200	> 200
Proximity to Road (meter)	<10	11-20	21-50	51-100	101-200	> 200
Proximity to Stream (meter)	<10	11-20	21-50	51-100	101-200	> 200
Aspect	Flat	North	Northeast	East	Southeast	South
	Southwest	West	Northwest			

Notes: the Southern Karakoram metamorphic Complex (SKm), the Hunza Plutonic Unit (HPU), the Shaksgam Formation (SF) and Quaternary (Q).

following Dahal et al. (2008b).

Proximity to road: The road network was digitized from the SPOT-5 image. These roads included all paved and unpaved roads. The major road in the Hunza valley is the Karakoram Highway (KKH). To evaluate the influence of roads and the distance to roads on landslide occurrences, the road network was classified into 6 buffer zones based on proximity, following (Dahal et al. 2008b) (Table 2).

Proximity to streams: Stream network in the study area was computed from the SRTM DEM with the hydrology tool in ArcGIS 10.2.2 software. Six buffer zones were created around every stream (Dahal et al. 2008b).

2.3 Correlation of landslides and landslide causative factors

To evaluate the importance of each causative factor for landslide susceptibility, the landslide inventory was compared to each of causative factors using the weight of evidence and frequency ratio modelling.

2.3.1Weight of evidence modelling

Weight of evidence statistical modelling is explained in Eqs. 1 and 2; a detailed description can be found in Bonham-Carter (1994) Bonham-Carter et al. (1989).

$$W^+ = In\frac{P(\frac{B}{D})}{P(\frac{B}{\bar{D}})} \quad (1)$$

$$W^- = In\frac{P(\frac{\bar{B}}{D})}{P(\frac{\bar{B}}{\bar{D}})} \quad (2)$$

where, P is the probability and ln is the natural log. B is the presence of a potential landslide evidence factor, $\bar{B}$ is the absence of potential landslide evidence factor. Similarly, D is the presence of landslide, while $\bar{D}$ is the absence of landslide.

To calculate the weights of each causative factor towards landslide distribution and occurrences, Eq. 3 and Eq. 4 defined by (van Westen et al. 2003) as:

$$W^+ = In\{(\frac{[Npix_1]}{[Npix_1]+[Npix_2]})/(\frac{[Npix_3]}{[Npix_3]+[Npix_4]})\} \quad (3)$$

$$W^- = In\{(\frac{Npix_2}{[Npix_1]+[Npix_2]})/(\frac{[Npix_4]}{[Npix_3]+[Npix_4]})\} \quad (4)$$

where, $Npix_1$ is the number of pixels representing the presence of both landslide causative factor and landslides; $Npix_2$ is the absence of landslides causative factor and presences of landslides; $Npix_3$ is the presence of landslides causative factor and absence of landslides; and $Npix_4$ is the absence of both landslides and landslides causative factor.

Final weight (W^c) was calculated by Eq. 5.

$$W^c = (W^+) - (W^-) \quad (5)$$

The weight contrast (W^c) is the difference between W^+ and W^- and reflects the overall spatial relationship of the causative factors and landslides.

2.3.2 Frequency ratio modelling

The influence of a causative factor on the spatial distribution of landslides was also assessed by frequency ratio (FR) statistical modelling. Frequency ratio is the ratio of the area where landslides occurred in the study area, and is also the ratio of the probabilities of a landslide occurrence to a non-occurrence for a given attribute (Bonham-Carter 1994). The frequency ratio is calculated by using Eq. 6.

$$FR = \frac{Di/Ai}{\sum Di/\sum Ai} \quad (6)$$

where, Di is the area of landslides in the given class; Ai is the area of class; $\sum Di$ is the total sum of landslide in the entire study area; and $\sum Ai$ is the sum of the entire study area.

2.4 Development of landslide susceptibility index maps

Landslide susceptibility index maps were computed by overlaying the causative factors using Eq. 7 (Pradhan et al. 2010) after assigning a weight (W^c) to each factor:

$$LSI = \sum W^c \quad (7)$$

where, W^c is total derived weight of each factor.

The susceptibility index obtained from the frequency ratio value was summed to the developed landslide susceptibility index map using following equation:

$$LSI = \sum FR \quad (8)$$

To check the predictive power of different evidential parameters (Pradhan et al. 2010), four models with different combinations of evidential factors were generated for landslide susceptibility index maps using Eq. 7.

2.5 Validation of the results and modelling prediction power

The LSI maps were verified by a success rate

curve, and a prediction rate curve was used to validate the prediction power of the models (Dahal et al. 2008a; Neuhäuser et al. 2012). The success rate curve was calculated by comparing the modelling landslides set with LSI map, following Mezughi et al. (2011) and Xu et al. (2012). The resultant LSI layer weights were divided into 100 classes with 1% cumulative intervals, ranging from high-susceptible to non-susceptible (Mezughi et al. 2011). These 100 classes were combined with the landslide inventory to find the percentage of landslide occurrences in each susceptible class. Similar to the success rate curve approach, a prediction rate curve was calculated, where the validation set of the landslide inventory was used as input.

2.6 Classification of landslide LSI map

The final LSI map was classified into five susceptibility zones (Mezughi et al. 2011), ranging from "very low" to "very high", according to the prediction rate curve (Dahal et al. 2008a). This classification scheme is based on the natural break law of the success rate curve distribution weight values frequency (Regmi et al. 2010; Xu et al. 2012). Finally, the accuracy of landslide susceptibility map was assessed by comparing the percentage area covered by each susceptibility class with the percentage of area covered by a landslide occurrence in each class.

3 Results

3.1 Landslide inventory

A total of 172 landslides were mapped in the study area (Figure 5). Out of these landslides, 13 have a relatively large of >0.95 km², and the

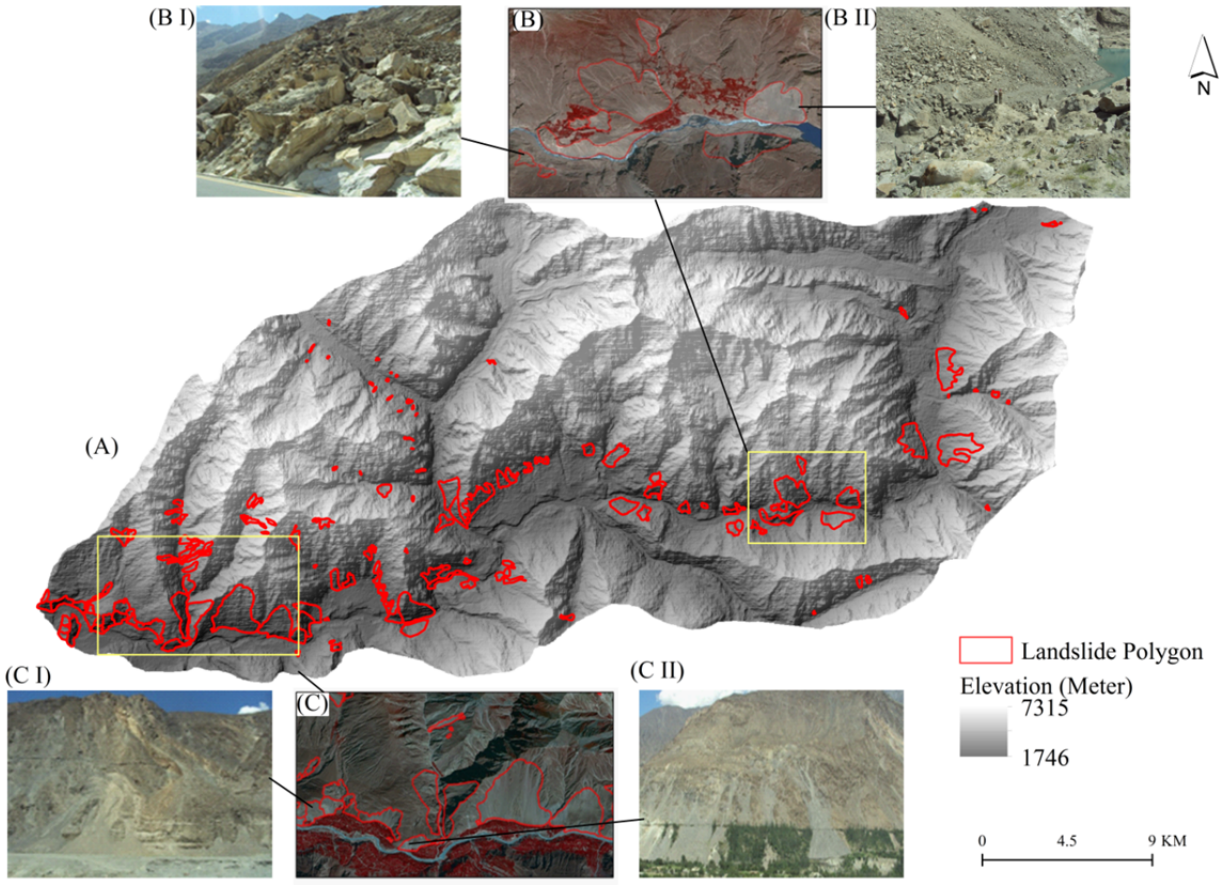

Figure 5 (A) shows the landslide inventory of the study area shown on the SRTM DEM, (B) and (C) are zoomed-in sections showing landslide polygons on the SPOT-5 image. (BI) is a picture of a rock slide at the Karakoram Highway road side. (BII) shows a landslide which blocked the Hunza river and created the Atta Abad lake. (CI) and (CII) show debris flows at Hussain Abad and Maiun, respectively.

remaining 159 landslides have an area of <1 km². The smallest landslide in the area has an area of only 6 m². The mapped landslides were randomly classified into a model calibration set (137, as 80%) and a model validation set (35, as 20%) (Figure 6).

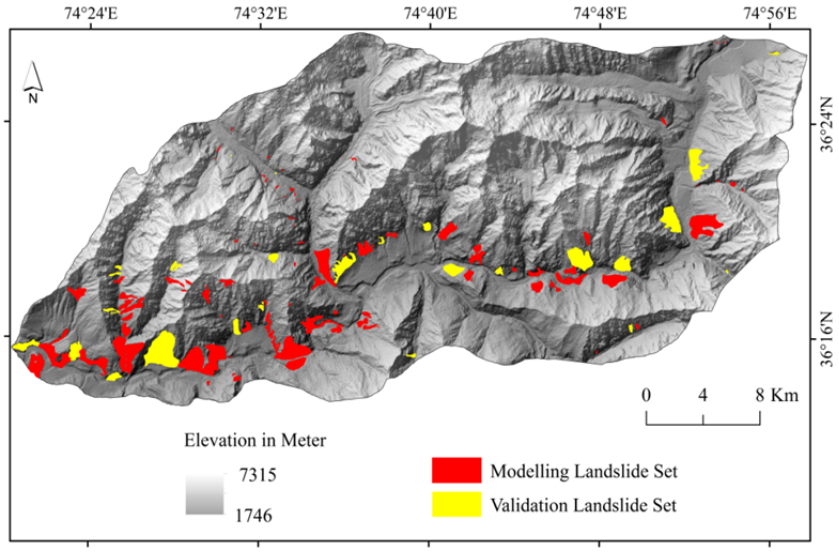

Figure 6 The modelling and validation landslide set. The modelling set was used for landslide susceptibility mapping, while the validation landslide set was used for validation of the modelling.

3.2 Description of factors weighting

The spatial distribution of landslides is controlled by causative factors (Zhuang et al. 2015) which are shown in Figure 7. The weight and ratio for each causative factor was calculated by correlating the landslide modelling set with the causative factors. The positive (W^+), negative (W^-), contrast (W^c) weights and the frequency ratio (FR) were calculated for each causative landslide factor (Table 3). The descriptions of the calculated weight and ratios are as follows:

Slope and Aspect: The distribution of slope and aspect is shown in Figures 7a and 7c, respectively. The area covered by each class is shown in Table 3. In case a slope has an angle between 30° and 50°, the slope gradient shows a positive correlation with weight (W^c) of 0.1, 0.3 and 0.2, respectively. For terrain sloping 60° or more, the W^c is -0.2 and -0.6. Terrain with a Southern aspect has the highest W^c of 0.7. The lowest and negative correlation was observed with aspects to the North, Northwest, East and Northeast. The 30°, 40° and 50° slope angles show higher frequency ratios of 1.10, 1.32, and 1.19, respectively, and the frequency ratio for slopes less than 30° or greater than 60° shows the lowest value. The highest frequency ratio was calculated for South and Southwest facing slopes. North, Northeast and Northwest facing slopes shows the lowest frequency ratio of 0.46, 0.49 and 0.48, respectively.

Land cover: Barren land (Figure 7b) has the highest positive weight of 3.9 and frequency ratio of 1.8 and hosts 98.2 % of the landslide area (Table 3). Other land cover classes, i.e. agriculture, forest and grass land, show a negative weight and lowest frequency ratio value (Table 3) and these classes are thus less susceptible to landslides.

Geology: The Southern Karakoram Metamorphic Complex formation got the highest weight and frequency ratio of 1.9 and 1.8, respectively and hosts 85.6% of the landslide area. The lowest weight (-3.4) and lowest frequency ratio (0.04) was observed in the Shaksgam Formation (SF) (Table 3).

Proximity to road: Generally, landslide susceptibility decreases as distance from roads increases. It is evident from the calculated weight and frequency ratio, that the class of <10 m to 200 m distance show the highest positive weights and thus have a positive correlation. Within a proximity of <10 meter, landslide occurrence have a positive weight (1.7) and highest frequency ratio (1.7). Beyond 200 meter distance, the weight is negative (-0.8) and also the frequency ratio (0.97) is the lowest (Table 3).

Proximity to faults: The highest weight (1.9) and frequency ratio (1.7) was calculated for the class that represents < 10 meter distance from faults. The lowest negative weight (-0.41) was found for the class that represents > 200 meter distance. Up to 200 meter distance, the calculated weight is positive and has highest frequency ratio, while beyond 200 meter, the total calculated weight is negative (-1.1) (Table 3) and has also the

lowest frequency ratio value.

Proximity to streams: It is evident from Table 3 that the calculated weight and frequency ratio decrease as the distance from stream increases.

3.3 Landslide Susceptibility Index Maps

The weights and frequencies of factors in Table 3 are combined, using Eqs. 7 and 8, to create LSI maps. To evaluate the predictive power of the selected combination of evidential parameters, four different combinations of factors were used (Table 4). Figure 8 shows the four resulting landslide susceptibility index maps.

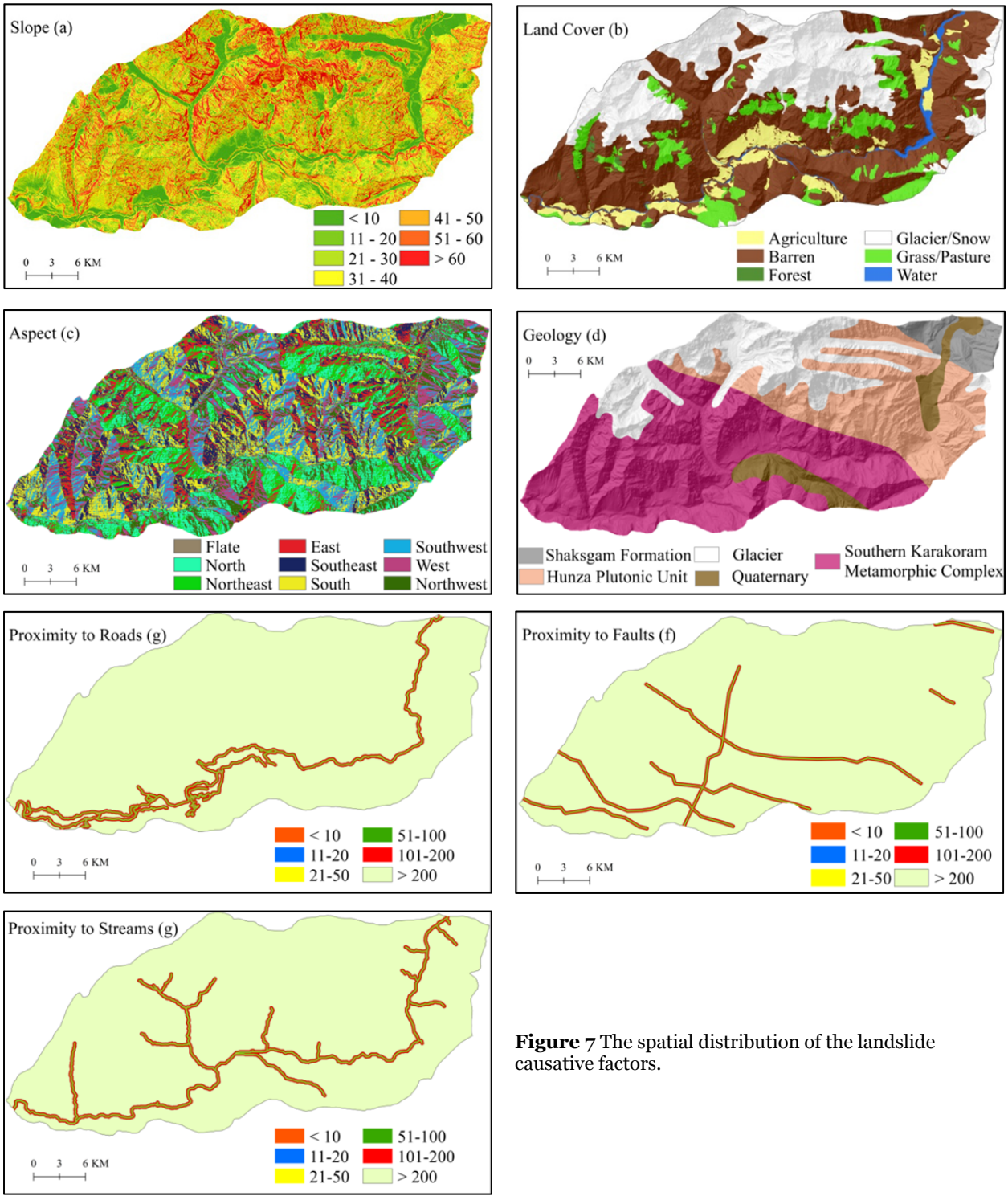

Figure 7 The spatial distribution of the landslide causative factors.

Table 3 Calculated weight of each class of causative factor

Parameter	Class	No. of Pixel in each class	% of Class	No. of Landslide Pixel in class	% of Landslide	W^+	W^-	W^c	FR
Aspect	Flat	72	0.01	0	0.00	0.00	0.00	0.00	0.00
	North	160073	12.29	3280	5.62	-1.64	0.07	-1.71	0.46
	Northeast	139800	10.74	3041	5.21	-0.75	0.06	-0.81	0.49
	East	148723	11.42	5510	9.44	-0.20	0.02	-0.22	0.83
	Southeast	177170	13.61	8754	15.00	0.10	-0.02	0.12	1.10
	South	199463	15.32	15656	26.82	0.60	-0.15	0.75	1.75
	Southwest	183224	14.07	11090	19.00	0.32	-0.06	0.38	1.35
	West	155873	11.97	8054	13.80	0.15	-0.02	0.17	1.15
	Northwest	137642	10.57	2990	5.12	-0.75	0.06	-0.81	0.48
Proximity to Fault (meter)	0-10	18985	1.46	1423	2.44	0.55	-0.01	0.56	1.67
	11-20	20035	1.54	1299	2.23	0.39	-0.01	0.40	1.45
	21-50	28036	2.15	1790	3.07	0.37	-0.01	0.38	1.43
	51-100	32201	2.47	1985	3.40	0.34	-0.01	0.35	1.38
	101-200	30395	2.33	1669	2.86	0.21	-0.01	0.22	1.23
	> 200	1172388	90.04	50209	86.01	-0.05	0.36	-0.41	0.96
Geology	Quaternary	77256	5.93	2960	5.07	-0.17	0.01	-0.18	0.85
	H P U	294010	22.58	5384	9.22	-0.93	0.17	-1.10	0.41
	S F	52060	4.00	86	0.15	-3.41	0.04	-3.45	0.04
	SKm	626270	48.10	49945	85.56	0.61	-1.30	1.91	1.78
Land Cover	Agriculture	93596	7.19	473	0.81	-2.22	0.07	-2.29	0.11
	Barren	694075	53.31	57340	98.23	0.65	-3.25	3.90	1.84
	Forest	5098	0.39	68	0.12	-1.59	0.00	-1.59	0.31
	Grass	134883	10.36	494	0.85	-2.59	0.11	-2.69	0.08
Proximity to Road (meter)	0 -10	11311	0.87	862	1.48	0.56	-0.01	0.57	1.70
	11-20	14199	1.09	994	1.70	0.47	-0.01	0.48	1.56
	21-50	16842	1.29	1120	1.92	0.42	-0.01	0.42	1.49
	51-100	22569	1.73	1377	2.36	0.33	-0.01	0.33	1.36
	101-200	36216	2.78	2041	3.50	0.24	-0.01	0.25	1.26
	> 200	1200903	92.23	51981	89.05	-0.04	0.36	-0.40	0.97
Slope (°)	< 10	98248	7.55	1068	1.83	-1.45	0.06	-1.52	0.24
	11-20	158720	12.19	4485	7.68	-0.48	0.05	-0.54	0.63
	21-30	228805	17.57	11254	19.28	0.07	-0.02	0.10	1.10
	31-40	324501	24.92	19243	32.96	0.26	-0.11	0.37	1.32
	41-50	292830	22.49	15653	26.81	0.15	-0.05	0.21	1.19
	51-60	155847	11.97	5665	9.70	-0.22	0.03	-0.26	0.81
	> 60	43089	3.31	1007	1.73	-0.67	0.02	-0.69	0.52
Proximity to Stream (meter)	< 10	14108	1.08	1098	1.88	0.59	-0.01	0.60	1.74
	11-20	17210	1.32	1290	2.21	0.55	-0.01	0.56	1.67
	21-50	18106	1.39	975	1.67	0.19	-0.01	0.20	1.20
	51-100	19438	1.49	971	1.66	0.11	-0.01	0.12	1.11
	101-200	42685	3.28	2099	3.60	0.10	-0.01	0.11	1.10
	> 200	1190493	91.43	51942	88.98	-0.03	0.27	-0.29	0.97

Table 4 Combination of causative factors and area under curve (AUC) in percentage. FR is frequency ratio.

Model	Factors Combination	AUC (%)
A	All seven parameters (Aspect, Slope, Geology, Land cover, Proximity to Fault, Proximity to Road, Proximity to Stream)	82.55
B	Aspect, Geology, Land cover, Proximity to Road, Slope, Proximity to Stream	76.79
C	Aspect, Slope, Land cover, Proximity to Fault, Proximity to Stream	62.67
D	Aspect, Slope, Geology, Proximity to Fault, Proximity to Stream	56.34
FR	All seven parameters (Aspect, Slope, Geology, Land cover, Proximity to Fault, Proximity to Road, Proximity to Stream)	79.36

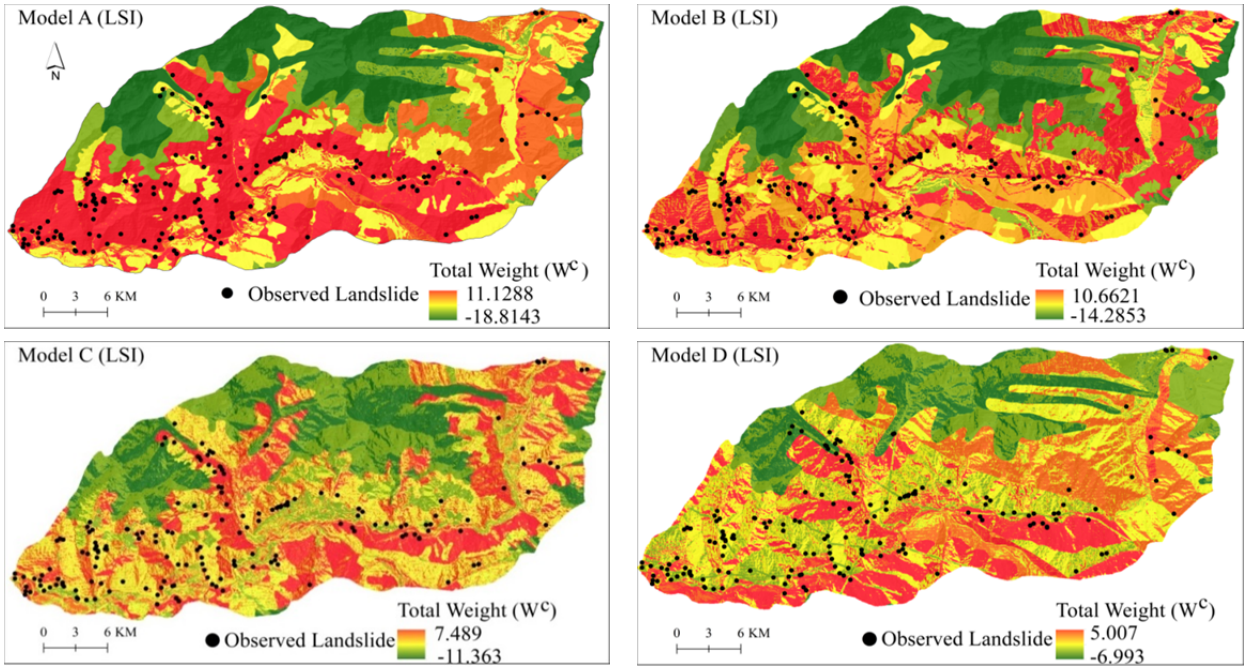

Figure 8 Landslide susceptibility index maps, with observed landslide locations in black dots, for different combinations of causative factors defined in Table 4.

3.4 Validation of the LSI maps

The LSI maps were verified by using a success rate curve. Success rate curves of all five models are shown in Figure 9. The success rate curve explains the accuracy rate of landslide occurrence and controlling factors using weight of evidence statistical modelling. Landslide susceptibility maps were also validated through the area under curve (AUC) criterion (Lee and Sambath 2006; Regmi et al. 2010). The area under curve (Table 4) criterion is a qualitative measurement of success rate values of the LSI maps, and was calculated from the success rate graphs (Figure 9) of each LSI. Model A, considering all causative factors, results in the highest obtained accuracy. We therefore selected Model A for landslide susceptibility mapping for the study area. Subsequently, the parameters used in Model A were also used in the FR model for susceptibility mapping. For Model A, the success rate curve (Figure 9) shows that 10% of the high susceptible areas have 59.1% of total observed landslide area, 30% of the high susceptible area has 77.9% of landslide area while 50% of the high susceptible area covers 87.5% of observed landslide area. Similarly for the FR

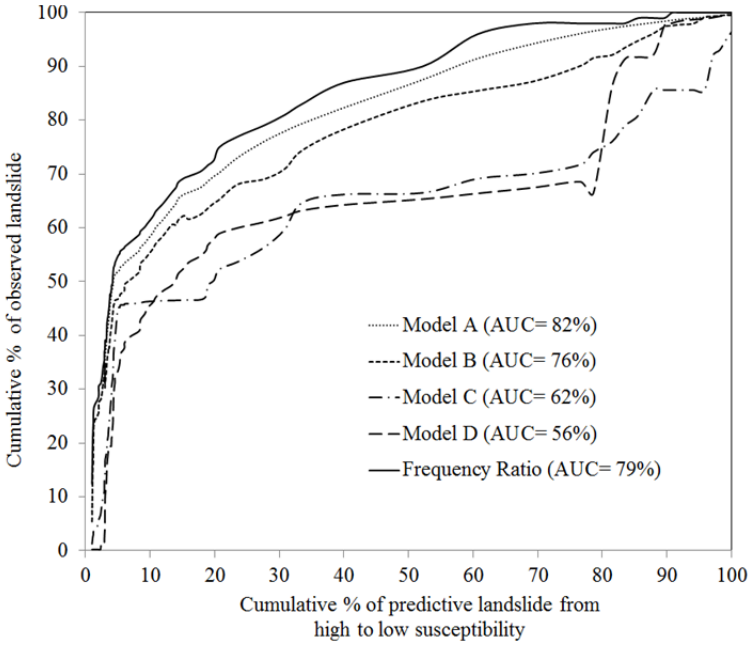

Figure 9 Success rate curves showing the prediction capacity of the four models and FR model and the area under curve (AUC). These curves were generated by crossing modelling landslide set (Figure 6) with LSI maps (Figure 8). Model A relatively predicts more landslides in the high susceptible classes.

Model, the success rate curve (Figure 9) shows that 10% of the high susceptible areas have 60.2% of the total observed landslide area, 30% of the high susceptible area has 80% of landslide area while 50% of the high susceptible area covers 89% of the observed landslide area.

3.5 Weight of evidence and Frequency ratio modelling prediction power

The prediction rate curve was used to validate the power of the modelling to predict future landslides (Dahal et al. 2008a; Neuhäuser et al. 2012). The prediction accuracy of Model A and the FR Model were evaluated. It appears that 10% of the highest susceptible area has 50.2% of the total observed landslide area, 30% of the highest susceptible area has 68.0% of landslide area while 50% of the highest susceptible area covers 79.2 % of the observed landslide area (Figure 10). Similarly, in the case of the FR Model, 10% of the highest susceptible area has 52.3% of the total observed landslide area, 30% of the highest susceptible area has 72% of landslide area while 50% of the highest susceptible area covers 81.4% of the observed landslide area (Figure 10).

3.6 Classified Susceptibility Map

Results show that Model A has a higher modelling and prediction rate compared to the other models. To provide a classified susceptibility map (Figure 11), model A was divided into five susceptible classes from "very low" to "very high", after (Mezughi et al. 2011). The classified landslide susceptibility map was validated by comparing landslide susceptible zone area with modelling landslide set area (Xu et al. 2012) (Figure 12). The "very high", "high" and "moderate" susceptibility zones are indeed covered by most of the landslides (Figure 12).

4 Discussion

The relative importance of each causative factor for landslide occurrences was investigated using weight of evidence and frequency ratio modelling, and is shown in Table 3. From this study, it appears that land cover and geology parameters have high W^c and FR values. These two factors are concluded to be the most important contributing factors for landslide occurrences in the study area which is also in agreement with Rahim et al. (2018). Generally, Bathrellos et al. (2009), Neuhäuser et al. (2012) and Neuhäuser and Terhorst (2007) also concluded that geology is the most important factor for landslide occurrences.

Moreover, of the geology parameter, the SKm (Southern Karakoram metamorphic Complex) class is more susceptible to landsliding, with highest W^c (1.9) and FR (1.8) values (Table 3). In the field, it was observed that the rocks of SKm are highly deformed, fractured, jointed and belongs to sediment productivity class, and inherently prone to slope failure (Rahim et al. 2018). While the Shaksgam Formation (SF), Hunza Plutonic Unit (HPU) and Quaternary were founded as low susceptibility classes (Table 3) which is also observed by Rahim et al. (2018). Faults present in the area are dormant since long time and therefore very few landslides are located close to the fault.

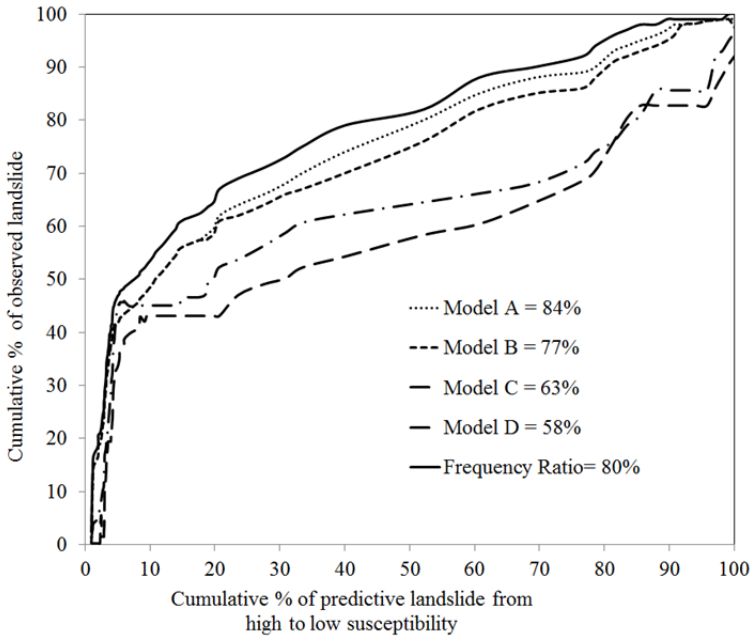

Figure 10 The prediction rate curves of four models and the FR model, showing the cumulated number of landslides captured by the susceptibility map (cumulated area) from high to low susceptibility classes. The prediction rate curve was calculated by crossing models landslide susceptibility map with the validation set of the landslide inventory.

Majority of the landslide occurred beyond 200 meter from faults (Table 3).

The barren class in land cover parameter is observed in high susceptibility class with highest calculated W^c (3.9) and FR (1.8) values (Table 3). The landslides were mapped from the SPOT-5 imagery and assigned to the land cover class "barren". This might have caused a feedback of the land cover class into the prediction of landslide locations. However, Malek et al. (2015) state that barren land is more prone to landslide occurrence due to direct exposure to climatic factors like, rain, snow and sun rays. On the other hand Reichenbach et al. (2014) stated that the presence of a vegetation cover prevents erosion of the soil surface and protects the surface from the weather, thus makes an area less prone to landsliding.

There is a close relationship of landslide

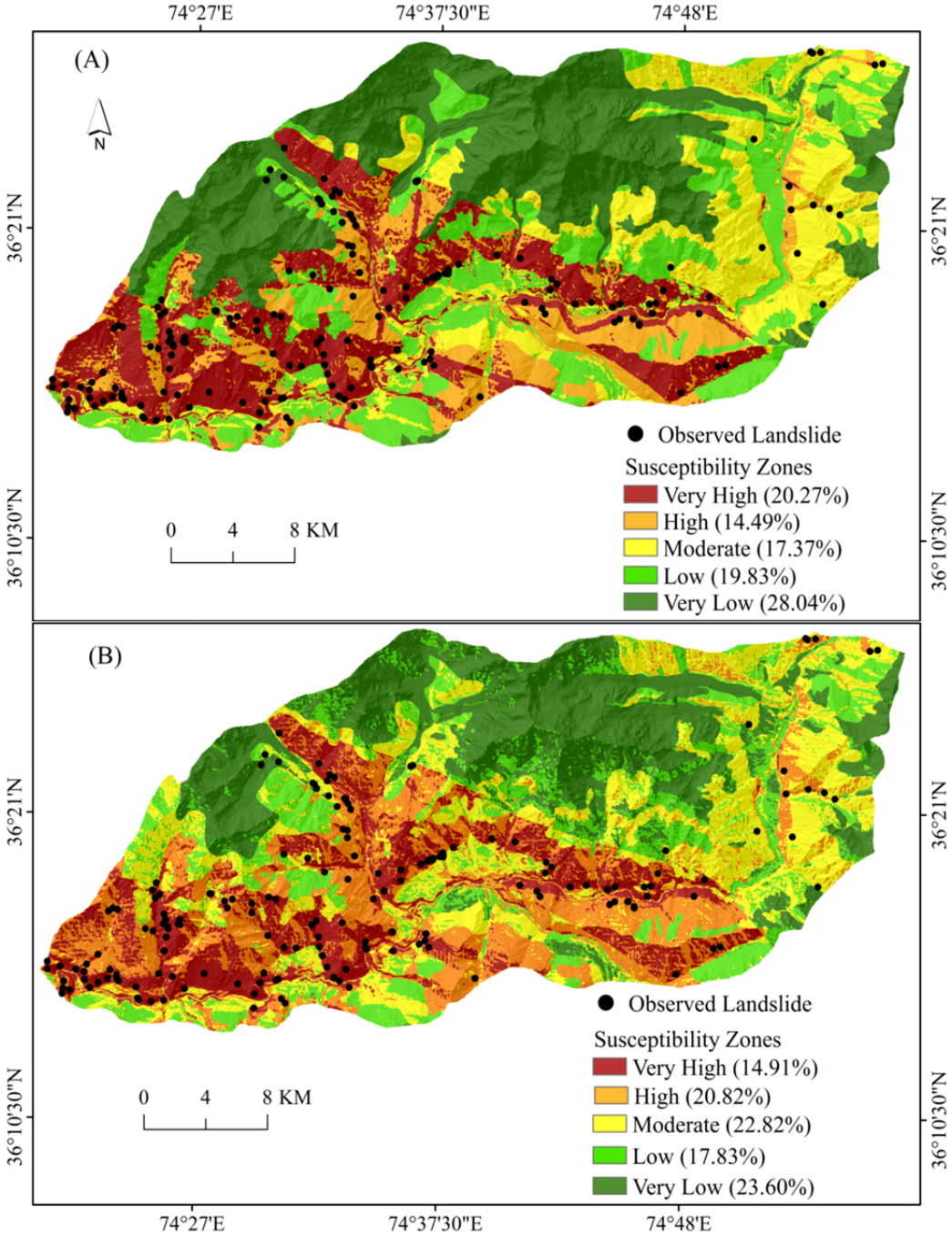

Figure 11 Landslide susceptibility zones of Model A (A) and the FR Model (B) showing susceptibility zones, with the area covered in percentage. The classification is based on the natural break law of prediction rate curve graph values.

susceptibility with the distance from roads and streams. It is clear from Table 3, that as the distance from road and stream increases, the landslide susceptibility decreases. This fact is also found in other studies, for examples, Pradhan et al. (2010) and Regmi et al. (2010). Slope cutting for road construction and the vibration produced by heavy traffic eventually results in land failure (Ayalew and Yamagishi 2005). In the Hunza- Nagar valley landslides along roads are not natural but triggered due to road construction. However, the 64% of landslides at far distance from the road are natural. Similarly, streams undercut slopes and the resulting erosion creates instability in the study area.

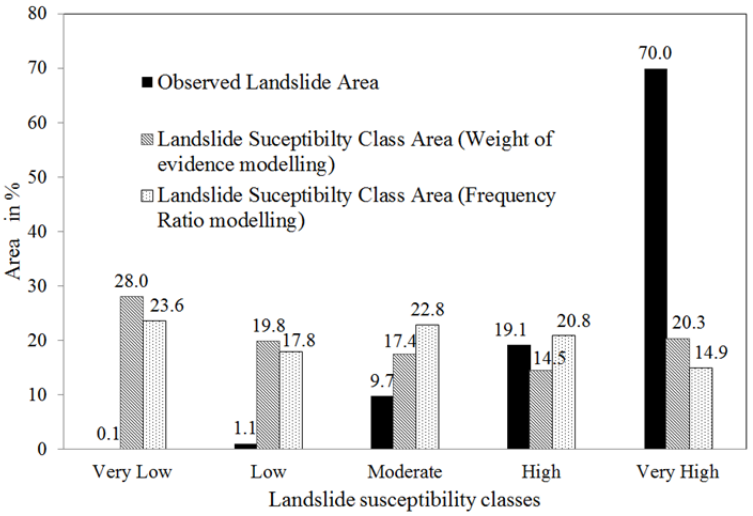

Figure 12 Validation of classified susceptibility maps, showing landslide susceptible zones and observed landslide area in percentage. Very high and high susceptibility zones are occupied by high concentration of observed landslides.

The results reveals, when the slope angles are between 30° and 50°, the W^c and FR is highest (Table 3), and therefore, are more susceptible to landslides. This favourable condition for landslides occurrences is also found by Dahal et al. (2008b). For slope angles of 60° and higher, the W^c is negative and the FR is lowest and is less susceptible (Table 3). The high steepness of such slopes lets detached material slide down instantly and accumulate at the toe, and no material is left on the slope to develop a landslide. However, such slopes are prone for rock or debris fall. South-facing slopes got highest W^c and FR values and are thus comparatively more susceptible to landsliding. This is also found by Xu et al. (2012). South-facing slopes are supposedly more exposed to the sun (Ren et al. 2013) and therefore more affected by chemical and mechanical weathering (De Guidi 2013). Earthquake is the major triggering factor of landslide. However, due to lack of data about seismic events and associated co-seismic landslides, we could not use earthquake as a variable in the susceptibility assessment.

Four different combinations of causative factors were tested for weight of evidence modelling (Table 4 and Figure 8). It is observed from the different combinations of factors and success rate curves (Figure 9), that the combination of aspect, slope, geology, land cover, proximity to fault, proximity to road and proximity to stream, is recommendable for landslide susceptibility assessment of this study area. Models C and D, without geology, land cover and proximity to road, shows less accuracy when compared to models A and B (Table 4 and Figure 9). The calculated prediction rate from both the weight of evidence and frequency ratio modelling is 84% and 80%, respectively. At the same time, the success rate curve shows 82% accuracy for weight of evidence modelling and 79% accuracy for the frequency ratio modelling. The prediction accuracy obtained from the weight of evidence modelling is comparable to previous studies such as Dahal et al. (2008b) (80%), Regmi et al. (2010) (78%) and Pradhan et al. (2010) (80%). The results of frequency ratio modelling from this study is very similar to other previous studies such that Mohammady et al. (2012) (80%) and Mezughi et al. (2011) (84%). From the present study the resultant susceptibility map accuracy (82%) produced by weight of evidence modelling is slightly higher (79%) than that of the map produced by frequency ratio.

From table 4 and figure 9 it can be seen that adding more landslide causative factors in the weight of evidence modelling leads to more accurate results. Moreover, in the weight of evidence and frequency ratio modelling, the resultant weighted value depends on the ratio between causative factor class area and the mapped

landslide area. If the landslide mapped area is larger than the class area, the resulting weight will be positive, and *vice versa*.

Weight of evidence modelling has some advantages: i) the methods provides a result based on weighted value rather than a subjective weight factor; ii) The prediction results are based purely on evidential parameters and therefore lead to reliable prediction results; and iii) the modelling can denote a well-tested technique for natural hazard study and spatial analysis. On the other hand, the weight of evidence modelling has some disadvantages, which was also pointed out by Regmi et al. (2010) i.e. the modelling overestimated the weight if the landslide are not evenly distributed and the area of factor class is very small.

In this study, we did not classify the landslides into different types and develop susceptibility map for all kinds of landslides. This is one of the limitations of the study. However, the landslide inventory map and susceptibility map developed in this study can be used for estimation of landslide hazard and risk assessment in the study area. The landslide susceptibility map can be used for site specific decision making tools, and can be used by local government for land use planning.

5 Conclusion

This paper presents a landslide inventory and landslide susceptibility map for the Hunza-Nagar valley in Northern Pakistan. Interpretation of a SPOT5 remote sensing image with field observations leads to an accurate identification of landslides in such an environment. The calculated weights (W^+, W^- and W^c) and frequency ratio values obtained with Bayesian probability modelling helped to determine the importance of seven causative factors for landslide occurrences. Geology, land cover, road and terrain slope are the major contributors for slope instability in the Hunza-Nagar valley. The results from weight of evidence modelling are better higher compared to frequency ratio results. We conclude that remote sensing derived data, supported with a GIS analysis and statistical modelling, perform well for landslide detection and landslide susceptibility mapping.

Acknowledgement

The authors thank the Pakistan Science Foundation (PSF) for providing financial support for the study.

References

Ahmed B (2015) Landslide susceptibility mapping using multi-criteria evaluation techniques in Chittagong Metropolitan Area, Bangladesh. Landslides 12(6): 1077-1095. https://doi.org/10.1007/s10346-014-0521-x

Akbar T, Ha SR (2011) Landslide hazard zoning along Himalayan Kaghan Valley of Pakistan—by integration of GPS, GIS, and remote sensing technology. Landslides 8(4): 527-540. https://doi.org/10.1007/s10346-011-0260-1

Ayalew L, Yamagishi H (2005) The application of GIS-based logistic regression for landslide susceptibility mapping in the Kakuda-Yahiko Mountains, Central Japan. Geomorphology 65(1): 15-31. https://doi.org/10.1016/j.geomorph.2004.06.010

Basharat M, Shah HR, Hameed N (2016) Landslide susceptibility mapping using GIS and weighted overlay method: a case study from NW Himalayas, Pakistan. Arabian Journal of Geosciences 9(4): 292. https://doi.org/10.1007/s12517-016-2308-y

Bathrellos GD, Kalivas D, Skilodimou HD (2009) GIS-based landslide susceptibility mapping models applied to natural and urban planning in Trikala, Central Greece. Estud Geol 65(1): 49-65. https://doi.org/10.3989/egeol.08642.036

Bonham-Carter GF (1994) Geographic Information Systems for geoscientists-modeling with GIS. Computer Methods In The Geoscientists 13398.

Bonham-Carter GF, Agterberg FP, Wright DF (1989) Weights of evidence modelling: a new approach to mapping mineral potential. Statistical Applications In The Earth Sciences 89(9): 171-183.

Booth AM, Roering JJ, Perron JT (2009) Automated landslide mapping using spectral analysis and high-resolution topographic data: Puget Sound lowlands, Washington, and Portland Hills, Oregon. Geomorphology 109(3–4): 132-147. https://doi.org/10.1016/j.geomorph.2009.02.027

Chalkias C, Ferentinou M, Polykretis C (2014) GIS-Based Landslide Susceptibility Mapping on the Peloponnese Peninsula, Greece. Geosciences 4(3): 176-190. https://doi.org/10.3390/geosciences4030176

Chau KT, Chan JE (2005) Regional bias of landslide data in generating susceptibility maps using logistic regression: Case of Hong Kong Island. Landslides 2(4): 280-290. https://doi.org/10.1007/s10346-005-0024-x

Chauhan S, Sharma M, Arora MK, Gupta NK (2010) Landslide Susceptibility Zonation through ratings derived from Artificial Neural Network. International Journal of Applied Earth Observation and Geoinformation 12(5): 340-350. https://doi.org/10.1016/j.jag.2010.04.006

CRED (2016) Poverty and death: disaster mortality 1996-2015 http://cred.be/downloadFile.php?file=sites/default/files/CRED_Disaster_Mortality.pdf

Dahal RK, Hasegawa S, Nonomura A, et al. (2008a) Predictive modelling of rainfall-induced landslide hazard in the Lesser Himalaya of Nepal based on weights-of-evidence. Geomorphology 102(3–4): 496-510. https://doi.org/10.1016/j.geomorph.2008.05.041

Dahal RK, Hasegawa S, Nonomura A, et al. (2008b) GIS-based weights-of-evidence modelling of rainfall-induced landslides

in small catchments for landslide susceptibility mapping. Environmental Geology 54(2): 311-324. https://doi.org/10.1007/s00254-007-0818-3
De Guidi G (2013) Landslide susceptibility assessment in the Peloritani Mts.(Sicily, Italy) and clues for tectonic control of relief processes. Natural Hazards and Earth System Sciences 13(4): 949. https://doi.org/10.5194/nhess-13-949-2013
Demir G, Aytekin M, Akgün A, et al. (2013) A comparison of landslide susceptibility mapping of the eastern part of the North Anatolian Fault Zone (Turkey) by likelihood-frequency ratio and analytic hierarchy process methods. Natural Hazards 65(3): 1481-1506. https://doi.org/10.1007/s11069-012-0418-8
Derbyshire E, Fort M, Owen LA (2001) Geomorphological Hazards along the Karakoram Highway: Khunjerab Pass to the Gilgit River, Northernmost Pakistan. Erdkunde 49-71. http://www.jstor.org/stable/25647347
Erener A, Mutlu A, Düzgün HS (2016) A comparative study for landslide susceptibility mapping using GIS-based multi-criteria decision analysis (MCDA), logistic regression (LR) and association rule mining (ARM). Engineering Geology 203: 45-55. https://doi.org/10.1016/j.enggeo.2015.09.007
Fell R, Corominas J, Bonnard C, et al. (2008) Guidelines for landslide susceptibility, hazard and risk zoning for land use planning. Engineering Geology 102(3–4): 85-98. https://doi.org/10.1016/j.enggeo.2008.03.022
Haeberlin Y, Turberg P, Retiere A, et al. (2004) Validation of Spot-5 satellite imagery for geological hazard identification and risk assessment for landslides, mud and debris flows in Matagalpa, Nicaragua. Nat. Resour. Canada 35(1): 273-278.
Hewitt K (1998) Catastrophic landslides and their effects on the Upper Indus streams, Karakoram Himalaya, northern Pakistan. Geomorphology 26(1): 47-80. https://doi.org/10.1016/S0169-555X(98)00051-8
Kamp U, Growley BJ, Khattak GA, Owen LA (2008) GIS-based landslide susceptibility mapping for the 2005 Kashmir earthquake region. Geomorphology 101(4): 631-642. https://doi.org/10.1016/j.geomorph.2008.03.003
Kanungo DP, Arora MK, Gupta RP, Sarkar S (2008) Landslide risk assessment using concepts of danger pixels and fuzzy set theory in Darjeeling Himalayas. Landslides 5(4): 407-416. https://doi.org/10.1007/s10346-008-0134-3
Kargel JS, Leonard G, Crippen RE, et al. (2010) Satellite Monitoring of Pakistan's Rockslide - Dammed Lake Gojal. Eos, Transactions American Geophysical Union 91(43): 394-395.
Kayastha P, Dhital MR, De Smedt F (2013) Application of the analytical hierarchy process (AHP) for landslide susceptibility mapping: A case study from the Tinau watershed, west Nepal. Computers & Geosciences 52(0): 398-408. https://doi.org/10.1016/j.cageo.2012.11.003
Khattak GA, Owen LA, Kamp U, Harp EL (2010) Evolution of earthquake-triggered landslides in the Kashmir Himalaya, northern Pakistan. Geomorphology 115(1): 102-108. https://doi.org/10.1016/j.geomorph.2009.09.035
Kumar KV, Martha T, Roy P (2006) Mapping damage in the Jammu and Kashmir caused by 8 October 2005 Mw 7.3 earthquake from the Cartosat–1 and Resourcesat–1 imagery. International Journal of Remote Sensing 27(20): 4449-4459. https://doi.org/10.1080/01431160600702376
Lee S, Choi J (2004) Landslide susceptibility mapping using GIS and the weight-of-evidence model. International Journal of Geographical Information Science 18(8): 789-814. https://doi.org/10.1080/13658810410001702003
Lee S, Pradhan B (2007) Landslide hazard mapping at Selangor, Malaysia using frequency ratio and logistic regression models. Landslides 4(1): 33-41. https://doi.org/10.1007/s10346-006-0047-y
Lee S, Sambath T (2006) Landslide susceptibility mapping in the Damrei Romel area, Cambodia using frequency ratio and logistic regression models. Environmental Geology 50(6): 847-855. https://doi.org/10.1007/s00254-006-0256-7
Lodhi MA (2011) Earthquake-induced landslide mapping in the western Himalayas using medium resolution ASTER imagery. International Journal of Remote Sensing 32(19): 5331-5346. https://doi.org/10.1080/01431161.2010.502158
Malek Ž, Zumpano V, Schröter D, et al. (2015). Scenarios of land cover change and landslide susceptibility: An example from the Buzau Subcarpathians, Romania. In: Lollino G, Manconi A, Guzzetti F, et al. (eds.), Engineering Geology for Society and Territory - Volume 5. Springer International Publishing. pp. 743-746.
Martha TR, Kerle N, Jetten V, et al. (2010) Characterising spectral, spatial and morphometric properties of landslides for semi-automatic detection using object-oriented methods. Geomorphology 116(1): 24-36. https://doi.org/10.1016/j.geomorph.2009.10.004
Martha TR, van Westen CJ, et al. (2013) Landslide hazard and risk assessment using semi-automatically created landslide inventories. Geomorphology 184: 139-150. https://doi.org/10.1016/j.geomorph.2012.12.001
Mathew J, Jha VK, Rawa GS (2007) Weights of evidence modelling for landslide hazard zonation mapping in part of Bhagirathi valley, Uttarakhand. Current Sciences 92(5): 628-638.
Mezughi TH, Akhir JM, Rafek AG, Abdullah I (2011) Landslide susceptibility assessment using frequency ratio model applied to an area along the E-W Highway (Gerik-Jeli). American Journal of Environmental Sciences 7 (1): 43-50.
Mohammady M, Pourghasemi H, Pradhan B (2012) Landslide susceptibility mapping at Golestan Province, Iran: A comparison between frequency ratio, Dempster-Shafer, and weights-of-evidence models. Journal of Asian Earth Sciences 61(0): 221-236. https://doi.org/10.1016/j.jseaes.2012.10.005
Neuhäuser B, Damm B, Terhorst B (2012) GIS-based assessment of landslide susceptibility on the base of the weights-of-evidence model. Landslides 9(4): 511-528. https://doi.org/10.1007/s10346-011-0305-5
Neuhäuser B, Terhorst B (2007) Landslide susceptibility assessment using “weights-of-evidence” applied to a study area at the Jurassic escarpment (SW-Germany). Geomorphology 86(1): 12-24. https://doi.org/10.1016/j.geomorph.2006.08.002
Palin R, Searle M, Waters D, et al. (2012) Combined thermobarometry and geochronology of peraluminous metapelites from the Karakoram metamorphic complex, North Pakistan; New insight into the tectonothermal evolution of the Baltoro and Hunza Valley regions. Journal of Metamorphic Geology 30(8): 793-820. https://doi.org/10.1111/j.1525-1314.2012.00999.x
Panzera F, Lombardo G, Monaco C, Di Stefano A (2015) Seismic site effects observed on sediments and basaltic lavas outcropping in a test site of Catania, Italy. Natural Hazards 79(1): 1-27. https://doi.org/10.1007/s11069-015-1822-7
Park S, Choi C, Kim B, Kim J (2013) Landslide susceptibility mapping using frequency ratio, analytic hierarchy process, logistic regression, and artificial neural network methods at the Inje area, Korea. Environmental Earth Sciences 68(5): 1443-1464. https://doi.org/10.1007/s12665-012-1842-5
Pourghasemi HR, Mohammady M, Pradhan B (2012) Landslide susceptibility mapping using index of entropy and conditional probability models in GIS: Safarood Basin, Iran. CATENA 97(0): 71-84. https://doi.org/10.1016/j.catena.2012.05.005
Pradhan B (2010) Landslide susceptibility mapping of a catchment area using frequency ratio, fuzzy logic and multivariate logistic regression approaches. Journal of the Indian Society of Remote Sensing 38(2): 301-320. https://doi.org/10.1007/s12524-010-0020-z
Pradhan B, Oh HJ, Buchroithner M (2010) Weights-of-evidence model applied to landslide susceptibility mapping in a tropical hilly area. Geomatics, Natural Hazards and Risk 1(3): 199-223. https://doi.org/10.1080/19475705.2010.498151
Quan HC, Lee BG (2012) GIS-based landslide susceptibility mapping using analytic hierarchy process and artificial neural

network in Jeju (Korea). KSCE Journal of Civil Engineering 16(7): 1258-1266. https://doi.org/10.1007/s12205-012-1242-0
Rahim I, Ali SM, Aslam M (2018) GIS Based landslide susceptibility mapping with application of analytical hierarchy process in District Ghizer, Gilgit Baltistan Pakistan. Journal of Geoscience and Environment Protection 6 (02): 34. https://doi.org/10.4236/gep.2018.62003.
Regmi NR, Giardino JR, Vitek JD (2010) Modeling susceptibility to landslides using the weight of evidence approach: Western Colorado, USA. Geomorphology 115(1–2): 172-187. https:// doi.org/10.1016/j.geomorph.2009.10.002
Reichenbach P, Busca C, Mondini AC, Rossi M (2014) The influence of land use change on landslide susceptibility zonation: the Briga Catchment test site (Messina, Italy). Environmental Management 54(6): 1372-1384. https://doi.org/10.1007/s00267-014-0357-0
Reis S, Yalcin A, Atasoy M, et al. (2012) Remote sensing and GIS-based landslide susceptibility mapping using frequency ratio and analytical hierarchy methods in Rize province (NE Turkey). Environmental Earth Sciences 66(7): 2063-2073. https://doi.org/10.1007/s12665-011-1432-y
Ren Z, Zhang Z, Dai F, et al. (2013) Co-seismic landslide topographic analysis based on multi-temporal DEM—A case study of the Wenchuan earthquake. SpringerPlus 2(1): 544.
Saba SB, van der Meijde M, van der Werff H (2010) Spatiotemporal landslide detection for the 2005 Kashmir earthquake region. Geomorphology 124(1): 17-25. https://doi.org/10.1016/j.geomorph.2010.07.026
Sarkar S, Kanungo DP, Patra AK, Kumar P (2008) GIS based spatial data analysis for landslide susceptibility mapping. Journal of Mountain Science 5(1): 52-62. https://doi.org/10.1007/s11629-008-0052-9
Scaioni M, Longoni L, Melillo V, Papini M (2014) Remote sensing for landslide investigations: An overview of recent achievements and perspectives. Remote Sensing 6(10): 9600-9652. https://doi.org/10.3390/rs6109600
Searle M, Khan MA (1996) Geological map of North Pakistan and adjacent areas of Northern Ladakh and Western Tibet, scale 1: 650,000: Oxford University, Oxford, England.
Searle M, Khan MA, Fraser J, et al. (1999) The tectonicevolution of the Kohistan Karakoram collision belt along the Karakoram Highway transect, north Pakistan. Tectonics 18(6): 929-949. https://doi.org/10.1029/1999TC900042
Shafique M,van der Meijde M, Khan MA (2016) A review of the 2005 Kashmir earthquake-induced landslides; from a remote sensing prospective. Journal of Asian Earth Sciences 11868-80. https:// doi.org/10.1016/j.jseaes.2016.01.002
Shahabi H,Hashim M, Ahmad B (2015) Remote sensing and GIS-based landslide susceptibility mapping using frequency ratio, logistic regression, and fuzzy logic methods at the central Zab basin, Iran. Environmental Earth Sciences 1-22. https://doi.org/10.1007/s12665-015-4028-0
Shaw R, Rahman A. (2015). Introduction and Approaches of Disaster Risk Reduction in Pakistan Disaster Risk Reduction Approaches in Pakistan. Springer. pp 3-29.
Talaei R (2014) Landslide susceptibility zonation mapping using logistic regression and its validation in Hashtchin Region, northwest of Iran. Journal of the Geological Society of India 84(1): 68-86. https://doi.org/10.1007/s12594-014-0111-5
USGS (2015) Shuttle Radar Topography Mission (SRTM) 1 Arc-Second Global. (https://earthexplorer.usgs.gov/, accessed on: 2015-06-25)
van Westen CJ, Rengers N, Soeters R (2003) Use of geomorphological information in indirect landslide susceptibility assessment. Natural Hazards 30(3): 399-419. https://doi.org/10.1023/B:NHAZ.0000007097.42735.9e
Wan S, Lei TC, Chou TY (2012) A landslide expert system: image classification through integration of data mining approaches for multi-category analysis. International Journal of Geographical Information Science 26(4): 747-770. https://doi.org/10.1080/13658816.2011.613397
Xu C, Xu X, Dai F, et al. (2012) Landslide hazard mapping using GIS and weight of evidence model in Qingshui River watershed of 2008 Wenchuan earthquake struck region. Journal of Earth Science 23(1): 97-120. https://doi.org/10.1007/s12583-012-0236-7
Zhuang J, Peng J, Iqbal J, et al. (2015) Identification of landslide spatial distribution and susceptibility assessment in relation to topography in the Xi'an Region, Shaanxi Province, China. Frontiers of Earth Science 9(3): 449-462. https://doi.org/10.1007/s11707-014-0474-3